Since January 2020 Elsevier has created a COVID-19 resource centre with free information in English and Mandarin on the novel coronavirus COVID-19. The COVID-19 resource centre is hosted on Elsevier Connect, the company's public news and information website.

Journal of Molecular Structure 1195 (2019) 208–219

Contents lists available at ScienceDirect

Journal of Molecular Structure

journal homepage: http://www.elsevier.com/locate/molstruc

Crystal structure, vibrational and optic properties of 2-N-methylamino-3-methylpyridine N-oxide – Its X-ray and spectroscopic studies as well as DFT quantum chemical calculations

I. Bryndal [a, *], J. Lorenc [b], L. Macalik [c], J. Michalski [b], W. Sąsiadek [b], T. Lis [d], J. Hanuza [c]

[a] Department of Drugs Technology, Faculty of Pharmacy with Division of Laboratory Diagnostics, Wroclaw Medical University, Borowska 211A, 50-556, Wrocław, Poland
[b] Department of Bioorganic Chemistry, Institute of Chemistry and Food Technology, Faculty of Engineering and Economics, Wrocław University of Economics, Komandorska 118/120, 53-345, Wrocław, Poland
[c] Institute of Low Temperature and Structure Research, Polish Academy of Sciences, Okólna 2, 50-422, Wrocław, Poland
[d] Faculty of Chemistry, University of Wroclaw, Joliot-Curie Street 14, 50-383, Wrocław, Poland

ARTICLE INFO

Article history:
Received 5 February 2019
Received in revised form
27 April 2019
Accepted 17 May 2019
Available online 24 May 2019

Keywords:
2-N-Methylamino-3-methylpyridine N-oxide
Synthesis
Crystal structure
IR
Raman
UV–Vis and luminescence spectra
NBO and DFT calculations

ABSTRACT

The crystal and molecular structure and physicochemical properties of 2-*N*-methylamino-3-methylpyridine *N*-oxide (MA3MPO) have been studied. MA3MPO was synthesized from 2-amino-3-methylpyridine by several steps to form colorless crystals suitable for crystallographic analysis. The data reveal that MA3MPO crystallizes in the monoclinic space group $P2_1/n$. The studied compound contains a nearly flat triply substituted pyridine skeleton whose structure is stabilized by an intramolecular N–H···O hydrogen bond. The N-oxide molecules are connected together by weak C–H···O hydrogen bonds, an acceptor of which is the oxygen atom from the N-oxide group. This leads to creation of two-dimensional network of hydrogen bonds. Its IR, Raman, UV–Vis and luminescence spectra have been measured and analyzed on the basis of DFT and NBO quantum chemical calculations in which the B3LYP/6-311++G(d,p) approach was applied. The distribution of the electron levels in the studied compound has been analyzed in terms of the possibility of its participation in the ligand-to-lanthanide ion energy transfer.

1. Introduction

Pyridine derivatives belong to the exceptional class of heterocyclic compounds due to the variety of their appearance in nature, and their applications in different areas. They form a prosthetic group of many enzymes that play a significant role in living organisms. They are present in vitamins, such as pyridoxine and niacin, as well as in natural alkaloid nicotine. Simple pyridine derivatives appear as metabolites from bacteria and fungi [1]. Nikkomycins [2], piericidins [3], collismycins [4] belong to this class of compounds. New bioactive bacteria metabolites and new natural vitamin B6 analogues were obtained from terrestrial *Streptomyces* sp. and characterized [5]. Due their biological activity, they form basic units in thousands of drugs, pharmaceuticals, antibiotics, insecticides and medically significant substances. Pyridine derivatives also possess anti-inflammatory [6,7], antiviral [8,9], anticancer [10–14], antimicrobial activity [15,16], antidiabetic [17,18], osteogenic [19,20], antihypertensive [21] and perfumery applications [22].

Very prospective applications of these compounds originate from their antiviral activity. It was found that they are active against HIV-1, HIV-2 and human cytomegalovirus (HCMV) as well as they show antifungal properties [23–30]. Pyridine N-oxides also show inhibiting properties against several coronaviruses which suggests the necessity of investigating them pre-clinically in the future as a potential new class of antiviral drugs [31].

The pyridine N-oxide derivatives form unique class of compounds are products of the pyridine oxidation. They are used frequently as oxidizing reagents in organic syntheses [32,33]. Another huge potential of pyridine N-oxides and their derivatives is related to the possibilities of complexation of metal ions by the oxygen atom of the N-oxide group. The potential mode of action

* Corresponding author.
E-mail address: iwona.bryndal@umed.wroc.pl (I. Bryndal).

https://doi.org/10.1016/j.molstruc.2019.05.064
0022-2860/

may include complexation of metal ions by the oxygen atom of heterocyclic N-oxides [34,35].

The present paper is a continuation of our studies on 2-aminopyridine derivatives [36–40] and their N-oxides [41,42]. Herein, we present the X-ray single crystal structure of 2-N-methylamino-3-methylpyridine N-oxide (MA3MPO) and the results of IR, Raman, UV–Vis and luminescence spectra, complemented by an analysis on the basis of the DFT and NBO quantum chemical calculations. Application of the density functional theory for assignment of the IR and Raman bands to the respective normal modes of vibrations is particularly valuable and credible when the input data for these calculations use the structural parameters derived from the XRD studies, as this was done in this work. This allowed for evaluation of vibrational and electron energy levels of the studied compound, their assignment to respective transitions between them, electron density of the atoms characterized by Mulliken population parameters derived from MPA analysis and non-bonding orbitals (NBO). Quantum chemical calculations were performed using the Gaussian 03W program and the B3LYP method broadly applied in chemistry. As in our earlier papers, the B3LYP/6-311++G (d,p) approach, that allows for comparison of the former [36–42] and present results, was used.

All these studies were undertaken to characterize the structural and spectroscopic properties of this kind of heterocyclic compounds, hoping that they can be used for complexation of the lanthanide ions which may form light emitting systems. The N-oxide group substituted to the pyridine ring can act effectively as an electron donor and electron acceptor at the same time. For these reasons, these compounds appear as synthetic intermediates in the field of heterocyclic chemistry, protecting groups, auxiliary agents, catalysts and as complexing ligands of d- and f-metal ions.

2. Experimental

2.1. Synthesis

2-N-Methylamino-3-methylpyridine N-oxide (MA3MPO) was synthesized from 2-amino-3-methylpyridine by means of several reactions shown in Fig. 1. The synthesis method leading to the 2-chloro-3-methylpyridine N-oxide was described earlier [43]. The last step of this synthesis was nucleophilic substitution of the chlorine atom in the 2 position by the methylamine group. 2-Chloro-4-nitropicoline N-oxide reacts with the primary amines under reflux in methanol solution to give the 2-N-alkylaminopyridine derivatives. Lack of nitro substituent in the 4-position of the 2-chloro-3-methylpyridine N-oxide causes that substitution of chlorine with methylamine in the methyl solution does not take place. The use of an aqueous solution of methylamine and heating the reaction mixture to 120 °C gives the expected product.

The reaction was carried out as follows: 5 g of 2-chloro-3-methylpyridine N-oxide and 10 g of 40% aqueous solution of methylamine were dissolved in 50 cm^3 of water. The mixture was placed in the autoclave and was heated for 5 h at 120 °C. Excess of methylamine and water was distilled off and allowed to crystallize. The result of this reaction, a colourless crystalline substance, was obtained in 63% yield. Its melting point equal to $m_p = 106$ °C (379 K).

The composition of the obtained compound was established by microanalysis giving the following stoichiometry: calculated C – 60.84%; N – 20.28%; H – 7.24%, found C – 60.40%; N – 19.99%; H – 7.25%.

2.2. Single crystal X-ray diffractions

A block-shaped colourless crystal of MA3MPO suitable for single-crystal X-ray diffraction analysis was obtained by recrystallization from a methanol/ethanol diffusion solvent system in the air at room temperature. Crystallographic measurement was performed on a Kuma KM4-CCD automated four-circle diffractometer with graphite monochromatized Mo Kα radiation at 110(2) K using an Oxford Cryosystems cooler. The CRYSALIS program system was used for data collection, cell refinement and data reduction [44]. The structure was solved by direct methods using the SHELXS-97 program [45], and refined on F^2 by full-matrix least squares with anisotropic thermal parameters for all non-H-atoms using SHELXL-97 [46]. All H-atoms were initially located in difference Fourier maps, and in the final refinement cycles were treated as described below. All C-bound H atoms were placed in the calculated positions, with C–H = 0.95–0.98 Å, and refined with the riding model with $U_{iso}(H) = 1.2U_{eq}(C)$ for CH or $1.5U_{eq}(C)$ for CH_3. The N-bonded H atom was refined freely, with $U_{iso}(H) = 1.2U_{eq}(N)$. The figures were made using the DIAMOND program [47]. Complete crystallographic data for the structural analysis have been deposited with the Cambridge Crystallographic Data Centre; CCDC reference number 1885627. These data can be obtained free of charge via www.ccdc.cam.ac.uk/conts/retrieving.html (or from the Cambridge Crystallographic Data Centre, 12 Union Road, Cambridge CB2 1EZ, UK; fax: (+44) 1223 336033; e-mail: deposit@ccdc.cam.uk).

Crystal data for MA3MPO: $C_7H_{10}N_2O$, $M_r = 138.17$, colorless block, crystal size 0.26 × 0.12 × 0.10 mm, monoclinic, space group $P2_1/n$, a = 8.099 (3), b = 8.995 (3), c = 10.128 (4) Å, β = 111.34 (4)°, $V = 687.2$ (5) $Å^3$, $T = 110(2)$ K, $Z = 4$, $\mu = 0.09$ mm^{-1} (for Mo K_α, λ = 0.71073 Å), 5965 reflections measured, 2266 unique (R_{int} = 0.025), 1649 observed ($I > 2\sigma(I)$), 96 parameters, 0 restraints, $R[F^2 > 2\sigma(F^2)] = 0.041$, $wR(F^2) = 0.116$, GOOF = $S = 1.05$, $(\Delta\rho_{max}) = 0.35$ and $(\Delta\rho_{min}) = -0.24$ e $Å^3$.

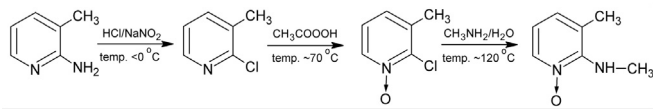

Fig. 1. The MA3MPO compound synthesis scheme.

2.3. IR and Raman studies

IR spectra were measured using the Nicolet iS50 FT-IR (Thermo Scientific) spectrometer equipped with an Automated Beamsplitter exchange system (iS50 ABX containing DLaTGS KBr detector and DLaTGS Solid Substrate detector for mid-IR and far-IR regions, respectively), built-in all-reflective diamond ATR module (iS50 ATR), Thermo Scientific Polaris™ and HeNe laser as an IR radiation source. The mid-IR spectra were collected in the 4000-100 cm^{-1} range in Nujol and Fluorolube mulls and KBr pellets. These spectra were compared to those recorded using the attenuated total reflection (ATR) technique with the advanced ATR correction software. This algorithm is a part of OMNIC™ 6.2 program attached to the Thermo Scientific Nicolet™ FT-IR spectrometer. The index of refraction was taken 1.5 characteristic for majority of organic materials. The ATR corrected IR spectra are identical to those obtained from transmission measurements [48]. The resolution of these measurements was 2.0 cm^{-1}.

Raman spectra (RS) in the 4000–80 cm^{-1} range were measured in back scattering geometry with a FT Bruker 110/S spectrometer. The resolution was 2.0 cm^{-1}. The YAG:Nd^{3+} laser operating at wavelength 1064 nm was used as an excitation source.

2.4. UV–Vis and luminescence studies

Room temperature electron absorption spectra were measured in the 200–1500 nm spectral range using a Cary-Varian 5E UV-VIS-near-IR spectrophotometer. The reflectance spectra were recorded with a Praying Mantis diffuse reflectance accessories. In these measurements, the base line was first recorded for the Al_2O_3 powder and, next, this line was subtracted from the obtained spectra for particular powder samples. The reflectance spectra were transformed into the absorption mode.

Excitation spectra were measured on a SSF-01 spectrofluorometer, equipped with PTI Felix software and ASOC 10 arrangement. The excitation source was a 150 W steady xenon lamp. Excitation spectra were corrected for the excitation light intensity.

Emission spectra were recorded with a grating spectrograph (Princeton Instr. Model Acton 2500i) coupled to a streak camera (Hamamatsu Model C5680) operating in the 200–1100 nm spectral range with temporal resolution of 20–100 ps.

2.5. Quantum chemical calculations

Geometry optimization of the studied compound was performed using Gaussian 03 program package [49], starting from X-ray geometry and applying the B3LYP approach [50–52] with the 6-311++G(d,p) basis set [53,54]. Its molecular structure and atomic description is presented in Fig. 2. Due to weak intermolecular interactions between the components of the unit cell, and the lack of factor group splitting in the experimental spectra, the calculations were performed for the monomeric molecule. The scaling factors were used to correct the evaluated wavenumbers for vibrational anharmonicity and deficiencies inherent to the used computational level. In the Potential Energy Distribution (PED) procedure the BALGA program was used [55]. The ChemCraft program was used for visualisation of the vectoring graphics of the normal modes [56]. The mean square deviation [57] between the experimental and calculated unscaled wavenumbers for MA3MPO was 7.7 cm^{-1} for the IR and 7.3 for the Raman spectra. The scaling of the calculated wavenumbers improves this result to 2.3 cm^{-1} for the IR and 2.7 for the Raman spectra. 0.9529 scaling factor was used for the range 3500–2500 cm^{-1} and 0.978 for the range 2499–0 cm^{-1} of the spectra. The theoretical Raman intensities were recalculated using the ChemCraft computer program.

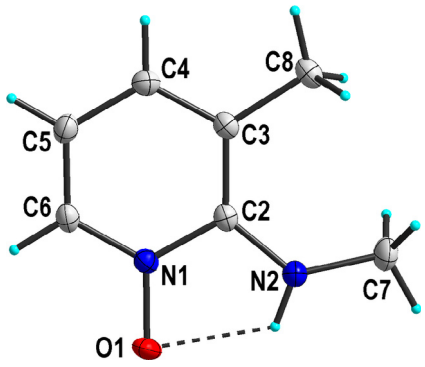

Fig. 2. The X-ray structure of MA3MPO, showing the atom-numbering scheme. Displacement ellipsoids are drawn at the 50% probability level and H atoms are shown as small spheres of arbitrary radii.

3. Results and discussion

3.1. Crystal structure

Table 1 lists selected geometrical parameters: bond lengths, bond angles and torsional angles. Experimental and calculated intra- and intermolecular hydrogen bonds as well as short contacts are compared in Table 2. The 2-N-methylamino-3-methylpyridine N-oxide (MA3MPO) crystallizes in the monoclinic space group $P2_1/n$ (Z = 4), with one symmetry-independent molecule in the asymmetric unit (Fig. 2). The pyridine ring in the crystal is almost planar (rms deviation of fitted atoms = 0.006 Å). Additionally, the methyl and the N-oxide groups lie almost within the pyridine ring plane. A slight distortion from this plane is observed for the N-methylamine group with torsion angles N1–C2–N2–C7 = 161.82 (9)° and C3–C2–N2–C7 = −21.05 (16)° (Table 1).

The N–O bond length of 1.3342 (11) Å is longer in comparison to the previously studied 2-alkylaminopyridine N-oxides, for which this value is within the range of 1.301(2)-1.318(2) Å [41,42,58–60]. Elongation of the N–O bond distance is most likely related to the involvement of the oxygen atom as a multiple acceptor for one intra- and three intermolecular hydrogen bonds (Table 2). Conformation of the MA3MPO molecule is stabilized by the intramolecular N–H···O [2.5266 (14) Å] hydrogen bond, between the hydrogen atom of the amine group and the oxygen atom of the NO group. Similar intramolecular hydrogen bond has been observed previously in these kinds of derivatives, and can be classified as medium strong [41,42,58–60].

The N-oxide molecules are connected together by three types of weak C–H···O hydrogen bonds. The first is created between the pyridine hydrogen and the oxygen atom from the N-oxide group [C4–H4···O1^{i} = 3.4147(17) Å; symmetry code: (i) x+1/2, -y+1/2, z+1/2]. The adjacent molecules are further joined by two other C–H···O interactions involving one of the H atoms of both methyl groups as donors and the oxygen atom of the N-oxide group as a double acceptor [C7–H71···O1^{ii} = 3.5340(18) Å and C8–H81···O1^{ii} = 3.2215(18) Å; symmetry code: (ii) -x+1/2, y-1/2, -z+1/2] (Table 2). This leads to creation of a two-dimensional network of hydrogen bonds in which the oxygen atom of the N-oxide group of each molecule occurs as a multiple acceptor (Fig. 3).

3.2. Vibrational data

Fig. 4 presents the theoretical and experimental IR and Raman spectra of the studied compound. Table 3 lists the observed and calculated wavenumbers together with their assignment to the respective normal modes based on PED data.

The X-Ray data obtained for the studied compound reveal that the amino and the N-oxide groups are nearly coplanar with the pyridine ring plane. Therefore, the molecular structure of this compound could be described by the C_s point group symmetry with the plane formed by pyridine ring, N=O bond and C–N–H(C–H) bonds of the N-methylamine group. 20 atoms of this molecule give rise to 60° of freedom that contain 3 rotational A' + 2A″ modes, 3 translational 2A' + A″ modes and 54 internal 35A' + 19A″ modes. The internal modes could be further subdivided into 18A' + 2A″ stretching and 17A' + 17 A″ bending modes. Because A' and A" modes are both IR and Raman active, 54 bands should be observed in both spectra. This is close to the number of bands seen in the IR spectrum (46 bands) and the Raman one (38 lines). Comparing these data, it is obvious that the Davidov splitting does not appear in our case and molecular C_s (and C_1) symmetry is sufficient in our considerations. Although the medium strong intramolecular N–H···O HB (D····A 2.527 Å) appears in the monomeric molecule (Fig. 2, Table 2), it does not influence the number of observed bands.

Table 1
Selected geometrical parameters (Å, °) for MA3MPO.

	Exp.	Calc.		Exp	Calc.
Distances					
O1—N1	1.3342 (11)	1.2978	C2—C3	1.4150 (14)	1.4065
N1—C6	1.3597 (13)	1.3601	C3—C4	1.3866 (14)	1.3971
N1—C2	1.3806 (13)	1.3951	C3—C8	1.5064 (15)	1.5099
N2—C2	1.3569 (13)	1.3731	C4—C5	1.4001 (15)	1.3942
N2—C7	1.4555 (14)	1.4591	C5—C6	1.3679 (15)	1.3812
Bond angles					
O1—N1—C6	119.60 (8)	120.79	C4—C3—C8	119.21 (9)	120.27
O1—N1—C2	117.97 (8)	118.60	C2—C3—C8	122.50 (9)	120.98
C6—N1—C2	122.43 (9)	120.61	C3—C4—C5	121.63 (10)	120.71
N2—C2—N1	112.50 (9)	112.20	C6—C5—C4	118.86 (9)	119.24
N2—C2—C3	128.91 (9)	128.13	N1—C6—C5	120.29 (9)	121.13
N1—C2—C3	118.54 (9)	119.56	C2—N2—C7	128.20 (9)	123.25
C4—C3—C2	118.22 (9)	118.68			
Torsion angles					
O1—N1—C2—N2	−0.22 (12)	−1.17	C2—C3—C4—C5	−0.82 (15)	1.76
C6—N1—C2—N2	179.16 (8)	178.63	C8—C3—C4—C5	−177.78 (9)	−175.32
O1—N1—C2—C3	−177.67 (7)	−177.74	C3—C4—C5—C6	0.84 (16)	0.45
C6—N1—C2—C3	1.70 (14)	2.06	O1—N1—C6—C5	177.64 (8)	180.00
N2—C2—C3—C4	−177.39 (9)	−178.95	C2—N1—C6—C5	−1.72 (15)	0.20
N1—C2—C3—C4	−0.41 (13)	−2.99	C4—C5—C6—N1	0.43 (15)	−1.46
N2—C2—C3—C8	−0.54 (15)	−1.90	N1—C2—N2—C7	161.82 (9)	137.45
N1—C2—C3—C8	176.44 (8)	174.06	C3—C2—N2—C7	−21.05 (16)	−46.34

Table 2
Intra- and intermolecular hydrogen bonds and short contacts (exp. and *calc.*) in MA3MPO.

D—H···*A*	*D*—H	H···*A*	*D*···A	*D*—H···*A*
N2—H2···O1	0.864 (12)	1.982 (12)	2.5266 (14)	119.9 (10)
	1.024	*1.893*	*2.539*	*117.9*
C4—H4···O1^{i}	0.95	2.48	3.4147 (17)	167
C7—H71···O1^{ii}	0.98	2.58	3.5340 (18)	165
C8—H81···O1^{ii}	0.98	2.31	3.2215 (18)	155

Symmetry codes: (i) $x+1/2, -y+1/2, z+1/2$; (ii) $-x+1/2, y-1/2, -z+1/2$.

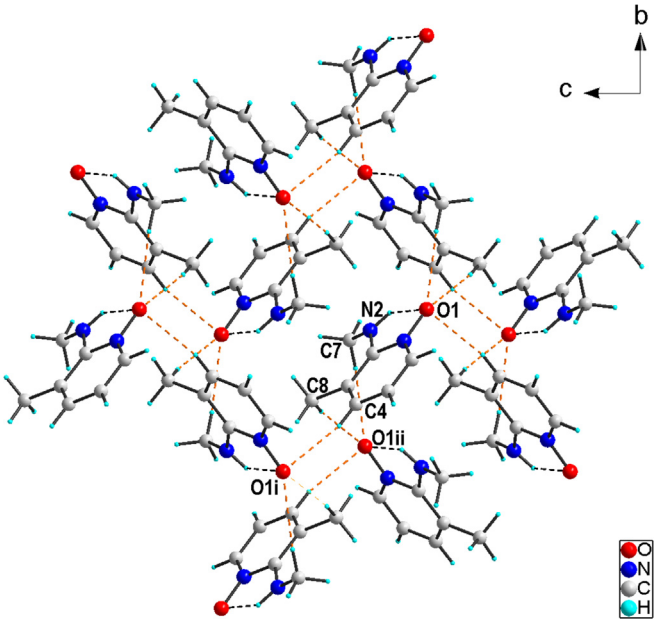

Fig. 3. The packing in the crystal structure of MA3MPO, viewed along the crystallographic ***a*** axis, showing the organization of molecules connected by C—H···O hydrogen bonds (orange dashed lines). Intramolecular N—H···O hydrogen bonds are marked with black dotted lines.

3.2.1. Pyridine ring and C—H vibrations

The assignment of the bands to the respective vibrations of pyridine rings was based on the nomenclature introduced by Urena et al. [61], Wilberg et al. [62] and our earlier studies of other pyridine derivatives [36–42]. The DFT calculations performed for the molecule studied here show that only few normal modes originate from the single coordinate. These are ν(NH), ν(CH), ν(CH$_3$), δ(CH$_3$) and τ(CH$_3$) vibrations. Other modes correspond to the concerted motions coupling few normal coordinates. The following ranges are proposed as pyridine ring modes: ν(CH): 3020–3090; ν(ϕ): 1580–1605; ν(ϕ)+ν(C$_\phi$-N): 1520-1535; δ(CH)+ν(ϕ): 1240–1325, 1140-1165, 1088-1105; δ(ϕ): 820–821; δ(ϕ)+ν(C$_\phi$-CH$_3$): ~689; γ(ϕ)+γ(N–O): 512-561 and ~396 cm^{-1}.

3.2.2. Methyl groups vibrations

The assignment of the methyl group vibrations was based on the DFT calculations presented here and the experimental data derived from our previous studies of other pyridine derivatives [36–42]. Three fundamental stretching ν_{as}(CH$_3$) bands are within the range of 2886–3005 cm^{-1} and those of ν_s(CH$_3$) are within the range of 2820–2876 cm^{-1}. Bending vibrations appear within the range of 1430–1484 cm^{-1} for δ_{as}(CH$_3$) modes and 1384-1422 cm^{-1} for δ_s(CH$_3$) modes. The other bands for the methyl groups' vibrations are observed in the following ranges: 956-1059 cm^{-1} for ρ(CH$_3$) rocking; 1240-1244 cm^{-1} for ν(ϕ-CH$_3$); 680-690 cm^{-1} for γ(ϕ-CH$_3$); 283-340 cm^{-1} for δ(ϕ-CH$_3$), and 120-230 cm^{-1} for τ(CH$_3$). In principle, the asymmetric and symmetric vibrations of the ring methyl group and attached to the amino group, described in Table 3 as (CH$_3$)a and (CH$_3$)b, lie within the same ranges, although the latter show a slight shift towards higher energy.

3.2.3. N—H vibrations

The assignment of the IR and Raman bands to the vibrations of the amino-group usually requires more attention. The vibrations of the C$_\phi$-N-H•••O moiety are described by 12° of freedom that includes 3 translations and 3 librations of the whole unit. Three of them refer to stretching vibrations and three correspond to the bending motions. However, due to the formation of the cyclic unit from the N-oxide and N—H groups, the number of modes in which the N—H bond is involved is significantly higher. The following,

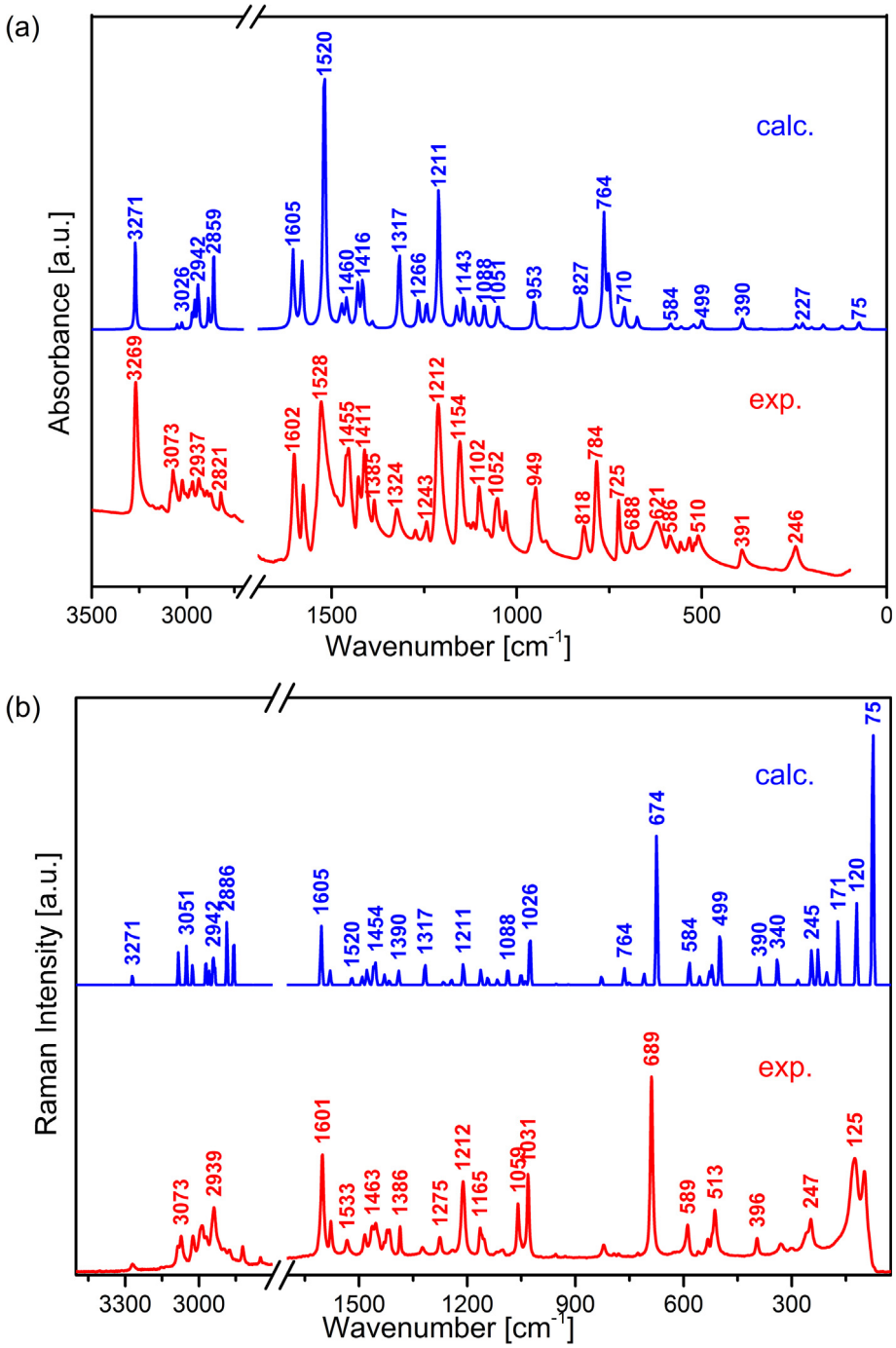

Fig. 4. Theoretical and experimental IR (**a**) and Raman (**b**) spectra of MA3MPO.

normal modes of this type have been recognized in the DFT calculations: ν(N-H_{HB}) at 3271 cm^{-1}; ρ(NH) and ρ(NH)+ν(ϕ) at 1478-1580 cm^{-1}; δ(ϕ)+ω(NH) at 764-827 cm^{-1} and τ(NHC) at 240-250 and 120-125 cm^{-1}. These vibrations appear at a somewhat lower wavenumbers than those originating from the NH bond not engaged in the hydrogen bonds. The shift of the NH_{HB} vibrational band depends on the HB bond strength and on the N–H···O angle. The smaller distance between the hydrogen donor and acceptor and the closer to 180°, the stronger bond and the greater band shift to the lower wavelengths [63,64].

3.2.4. N-oxide group vibrations

Due to the electron properties of this chromophore**,** the N-oxide group vibrations are strongly coupled with the vibrations of the pyridine ring. Therefore, they are involved in several vibrations observed in the whole MIR region. The following normal modes contain contribution of these motions: ν(NO) 1212-1324 cm^{-1}, δ(C_{ϕ}-N-O): 627-628 cm^{-1} and γ(NO): 395-571 and 171-227 cm^{-1} [41,42]. Such broad wavenumber range of these vibrations also follows the engagement of the oxygen atom of this group in the hydrogen bond. In derivatives containing a planar nitro group at the 4-position, the N–O bond of 1.301–1.305 and 1.315 Å length, mainly due to the return donation of the NO and NO_2 substituents, has the

Table 3
The proposed assignments of the IR and Raman bands to respective normal modes on the basis potential energy distribution (PED).

No	Calculated		Experimental		PED [%]
	IR, RS [cm^{-1}]	IR, RS [cm^{-1}] with fsc	IR[cm^{-1}]	RS[cm^{-1}]	
1	3436	3271(33;4)	3269vs	3271vw	ν(NH···O) −100
2	3239	3084(0;11)	3080vw	3085vw	νCH_{ϕ} −99
3	3205	3051(2;14)	3073w	3073vw	νCH_{ϕ} −99
4	3179	3026(2;8)	3024vw	3025vw	νCH_{ϕ} −99
5	3122	2972(6;9)	2981vw	2987vw	$\nu_{as}(CH_3)b$ −97
6	3108	2959(9;5)	2970vw	2971vw	$\nu_{as}CH_3a$ −97
7	3090	2942(15;11)	2937vw	2939w	$\nu_{as}CH_3b$ −85+ $\nu_{as}CH_3a$ −14
8	3084	2936(6;7)	2895vw	2899vw	$\nu_{as}CH_3a$ −85+ $\nu_{as}CH_3b$ −14
9	3032	2886(11;23)	2874vw	2876vw	ν_sCH_3a −99
10	3003	2859(29;18)	2821vw	2821vw	ν_sCH_3b −100
11	1641	1605(28;21)	1602s	1601m	$\nu\phi$ −62 + $\delta\phi$ −11+ δCH_{ϕ} −10
12	1616	1580(23;5)	1577m	1578w	$\nu\phi$ −59 + ρNH −19 + δCH_{ϕ} −11
13	1554	1520(100;3)	1528vs	1533vw	$\nu\phi$ −25 + $\nu C_{\phi}N$ −21 + ρNH −19 + δCH_{ϕ} −15
14	1525	1491(0;3)	1487sh	1484vw	$\delta_{as}CH_3b$ −52+ $\delta_{as}CH_3a$ −23
15	1511	1478(1;5)			ρNH −35 + $\nu\phi$ −28+ $\delta_{as}CH_3b$ −20 + δCH_{ϕ} −10
16	1506	1473(7;1)	1461w	1462w	$\delta_{as}CH_3a$ −42 +$\delta_{as}CH_3b$ −41 + δ_sCH_3b −13
17	1493	1460(9;6)	1455s	1454w	$\delta_{as}CH_3b$ −49 + $\delta_{as}CH_3a$ −46
18	1487	1454(1;8)	1428w	1430vw	$\delta_{as}CH_3a$ −71 + $\delta_{as}CH_3b$ −27
19	1462	1430(15;4)	1411s	1422vw	δ_sCH_3b −54 + δCH_{ϕ} −19 + $\nu\phi$ −11
20	1448	1416(17;2)		1416vw	δ_sCH_3b −25 + δCH_{ϕ} −25+ $\nu\phi$ −23 + $\delta_{as}CH_3a$ −16
21	1422	1390(2;5)	1385w	1386w	δ_sCH_3a −94
22	1347	1317(28;8)	1324w	1324vw	$\nu C_{\phi}N$ −23 + δCH_{ϕ} −25 + $\nu\phi$ −27 + νNO_{ϕ} −10
23	1294	1266(10;1)	1274vw	1275vw	δCH_{ϕ} −35+ $\nu\phi$ −27 + νNO_{ϕ} −18
24	1272	1244(9;2)	1243vw	1240vw	$\delta\phi$ −36 + νCCH_3a −21 + νNO_{ϕ} −11 + δCH_{ϕ} −11
25	1238	1211(51;8)	1212vs	1212m	$\nu\phi$ −54+ νNO_{ϕ} −9 + ρCH_3b −12
26	1188	1162(7;5)		1165w	ρCH_3b −32 + δCH_{ϕ} −26 + $\nu\phi$ −14 + νCCH_3a −10
27	1169	1143(11;3)	1154s	1154sh	δCH_{ϕ} −53 + ρCH_3b −21 + $\nu\phi$ −18
28	1141	1116 (8;2)	1117vw	1118vw	ρCH_3b −100
29	1112	1088(9;6)	1102m	1102vw	$\nu\phi$ −49 + δCH_{ϕ} −32
30	1074	1051(9;4)	1052w	1059w	νNCH_3b −43 + ρCH_3b −16 + $\delta\phi$ −17
31	1062	1038(1;2)	1030w	1031m	ρCH_3a −88
32	1049	1026(1;19)			ρCH_3a −49+ $\nu\phi$ −29
33	974	953(11;0)	949m	956vw	ρCH_3a −46+ $\nu\phi$ −24+ νNO_{ϕ} −11
34	940	920(0;0)	920vw		γCH_{ϕ} −83 + $\gamma\phi$ −17
35	891	871(0;0)			γCH_{ϕ} −85 + $\gamma\phi$ −12
36	846	827(12;3)	818w	821vw	$\delta\phi$ −46 + ωNH −17 + $\nu C_{\phi}N$ −10
37	782	764(40;6)	784s	794vw	ωNH −47+ $\tau NHCH_3b$ −25+ $\delta\phi$ −15
38	768	751(17;1)			γCH_{ϕ} −71 + $\gamma\phi$ −16
39	726	710(8;4)	725m	727vw	$\gamma\phi$ −63 + γCH_{ϕ} −17 + $\gamma\phi$N −10
40	689	674(4;56)	688w	689vs	$\nu\phi$ −51 + νCCH_3a −12 + $\nu C_{\phi}N$ −11 + $\delta\phi$NO −11
41	597	584(2;9)	621w	627vw	$\delta\phi$NO −26 + $\delta\phi$ −24 + $\delta\phi$N −14 + $\nu\phi$ −15
42	568	555(1;3)	586vw	589vw	$\gamma\phi$ −54 + $\delta\phi$ −7+ $\gamma\phi$N −16 + γCH_{ϕ} −14
43	541	529(1;5)	557vw	561vw	$\delta\phi$ −62 + $\delta\phi$NO −17 + $\delta\phi CH_3a$ −12
44	533	521(2;7)	533vw		$\gamma\phi$ −39 + $\gamma\phi$NO −22 + $\gamma\phi CH_3a$ −15
45	510	499(4;21)	510w	513w	$\delta\phi$ −51+ $\nu\phi$ −10 + νCCH_3a −10
46	399	390(4;6)	391w	396vw	$\delta\phi$ −25 + $\delta\phi$NO −21 + $\delta\phi$N −17
47	347	340(0;10)	330sh	332vw	$\delta\phi CH_3a$ −39 + $\gamma\phi$N −11 + $\gamma\phi CH_3a$ −11 + ρNH −10 + $\gamma\phi$ −10
48	289	283(0;2)	300sh	298vw	$\delta\phi CH_3a$ −31 + $\delta\phi$N −26 + $\gamma\phi$N −21
49	250	245(2;13)	246w	247w	ρNH−26+τCH_3b−16+$\delta\phi$N−14+$\gamma\phi CH_3a$−14+$\gamma\phi$N−10+$\tau NHCH_3b$−10
50	232	227(2;12)	221sh	224sh	$\gamma\phi CH_3a$ −43 + $\gamma\phi$ −27 + $\gamma\phi$NO −21
51	207	203(1;4)	201sh	201vw	τCH_3a −87
52	175	171(2;23)	164sh	172sh	τCH_3b −40 + $\gamma\phi$NO −17 + $\gamma\phi CH_3a$ −14 + ωNH −13 + $\gamma\phi$ −12
53	123	120(1;29)	127sh	125m	τCH_3b −42 + $\gamma\phi$N −18 + $\tau NHCH_3b$ −16
54	77	75(3;100)	103sh	98m	$\tau NHCH_3b$ −39 + ωNH −28 + $\gamma\phi$N −15 + $\gamma\phi$ −10

In-plane vibrations: ν – stretching; δ – bending; ρ – rocking; out-of-plane vibrations: γ – torsional; ω – wagging; τ – twisting; ϕ – pyridine ring. Used scaling factor: fsc = 0,9529 (4000–2000 cm^{-1}) and 0,978 (2000–30 cm^{-1}); a – pyridine methyl group; b – N-methylamine methyl group. Percentage of the intensity (IR;RS) is given in brackets.

double-bond character. In the molecule analyzed, the bond length of 1.334 Å indicates that the N–O bond is an almost single bond, and therefore its stretching vibration band should appear at lower wavenumbers. The second reason for the N–O bond elongation is the intramolecular interaction between the oxygen atom of the -NO and the hydrogen atom of the -$NHCH_3$ groups located at vicinal positions of the pyridine ring. For the above reasons, one should expect a shifting of this band toward red.

The characteristic stretching vibration of this bond is usually located within the range of 1200–1320 cm^{-1}. For the compound studied here, this vibration appears as a strong IR band and as a medium Raman band at 1212 cm^{-1}. Our theoretical calculations, presented in this paper, predict this vibration within the range of 1317 - 1212 cm^{-1} These values confirm the participation of the N-oxide group in medium strong intramolecular hydrogen bond as found in X-Ray studies. The comparison of selected geometrical parameters of the N-oxide intramolecular hydrogen bond and the respective wavenumbers of MA3MPO with 2-N-alkylamino-3-nitropyridine N-oxides [41,42] are presented in Table 4.

3.2.5. Intra- and intermolecular interactions

The complex contour in the 3200-3500 cm^{-1} range of the IR

spectrum and at about 3271 cm^{-1} of the Raman spectrum corresponds to the ν(NH) vibrations of the amino group. It contains two components because two types of N–H bond probably appear in this molecule: engaged and non-engaged in the HB-s. The D···A distance of the former system was determined in the crystal structure as 2.527 Å and angle 120°. Its theoretical value is close to experimental and equals 2.539 Å and 118°, respectively, and the visualisation contains an intramolecular hydrogen bond in the calculated molecule.

The ν(NH) vibrations are shifted from the theoretical values calculated for the isolated molecule at 3271 cm^{-1} (with scaling factor). Such shift agree with the HB theory described in the review by Bratos et al. [63].

The spectacular calculated stretching vibration of the O···H hydrogen bond, shown in Fig. 5 was found at 390 cm^{-1}. On the basis of the PED contributions, the experimental weak bands at 391 (396) cm^{-1} should be assigned to the stretching O···H vibration.

The X-ray studies propose the existence of additional C–H···O short contacts (c.a. 3.40 Å) between the oxygen atom of the N-oxide group and CH pyridine ring. The IR and Raman spectra and the quantum chemical calculations do not confirm the existence of such interactions between the adjacent molecules.

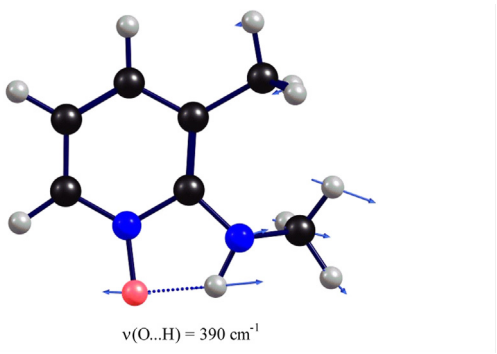

Fig. 5. The vibrational mode involving large contribution of stretching vibration of the O···H bond computed with the use of B3LYP model.

3.3. Electron absorption and emission spectra

3.3.1. Electronic properties of the studied compound

Two π-electron units compose the structure of the studied compound: pyridine ring and the N-oxide group. The latter unit can act both as an electron-donor and electron-acceptor in relation to the pyridine ring. The N-methylamino unit, situated at a position adjacent to the N-oxide group, is a typical electron-donor substituent.

Electron density of the atoms in this compound is characterized by Mulliken population parameters derived from the MPA analysis and non-bonding orbitals (NBO). Atomic charges and NBO data calculated using these procedures, are summarized in Table 5. The results of these calculations will be used in the discussion regarding the MA3MPO electron states.

While analyzing the MPA and NBO data, the following conclusions can be made:

- The polar character of N=O group showing positive NBO values of c.a. 0.02089 e on the nitrogen atom and negative value of c.a. −0.60156 e on the oxygen atom.
- Pyridine carbon atoms C2 and C6 have positive charges: 0.38951 and 0.02623 e, respectively. Negative charges appear for C3, C4 and C5 pyridine atoms, and their values are: −0.08966, −0.18571 and −0.25343 e, respectively.
- The negative values of Mulliken and NBO parameters were assigned for carbon atoms of the methyl groups, attached to the pyridine ring and amine group. The lower negative charge on the methyl group at C3 carbon of the pyridine ring originates from the electron-withdrawing effect of the pyridine ring (see Table 5).

Table 5
Mulliken population and NBO atomic charges parameters calculated for MA3MPO. Atomic numbering in this table is the same as shown in Fig. 2.

Atom No	Milliken	NBO
O1	−0.17357	−0.60156
N1	−0.190654	0.02089
C2	−0.938422	0.38951
C3	1.039825	−0.08966
C4	0.020341	−0.18571
H4	0.143455	0.20596
C5	−0.304130	−0.25343
H5	0.177985	0.21792
C6	−0.007052	0.02623
H6	0.206644	0.22171
N2	−0.127876	−0.63651
H2	0.296416	0.42298
C7	−0.360124	−0.35680
H71	0.161993	0.17883
H72	0.156806	0.20305
H73	0.144489	0.18738
C8	−0.744088	−0.58779
H81	0.162672	0.21172
H82	0.181033	0.21500
H83	0.154253	0.21031

Table 4
Comparison of selected geometrical parameters of the N-oxide intramolecular hydrogen bond, and the respective wavenumbers of MA3MPO with 2-N-alkylaminopyridine N-oxides [41,42]*.

Compound	$d(N–O)_{NO}$ (Å)		ν(N–O) (cm^{-1})		$d(N···O)_{HB}$ (Å) [<DHA (°)]		$\nu(N–H)_{HB}$ (cm^{-1})	
	exp. X-ray	calc.	exp. IR (RS)	calc.	exp.	cal.	exp. IR(RS)	calc.
2-N-methylamine-3-methylpyridine N-oxide (MA3MPO)	1.3342 (11)	1.298	1212 (1212)	1211	2.5266 (14) [119.9 (10)]	2.539 [117.9]	3271 (3272)	3271
2-N-ethylamino-3-methyl-4-nitropyridine N-oxide [42]	1.301 (2)	1.287	1308 (1308) 1226 (1229)	1295** 1262	2.491(3) [109.3 (11)]	2.565 [115.1]	3225 (3231)	3305
2-N-ethylamino-5-methyl-4-nitropyridine N-oxide [42]	1.3046(13)	1.288	1319 (1319) 1236 (1235)	1350** 1230	2.571 (2) [110.6 (11)]	2.558 [108.6]	3338 (3338)	3367
2-N-ethylamino-4-nitropyridine N-oxide [41]	1.3153(13) 1.3137(12)	1.249	1234 (1233)	1235	2.576 (2) [106.3 (1)] 2.554 (2) [90.4 (1)]	2.555 [109.22]	3297 (–) 3224 (–)	3336

*In Refs. [41,42], the intermolecular N–H···O hydrogen bonds were also found engaging N-oxide group as a donor; **stretching vibration of the NO bond coupled with symmetric vibration of the NO_2 group.

- Similar behavior should be noted in the case of charges on nitrogen atoms of the amino group, for which the NBO charge (−0.63651 e) is significantly higher than Mulliken value (−0.127876 e).
- The hydrogen atom of the methylamino group, interacting with the HB oxygen of N-oxide group, exhibits the highest positive charge (+0.42298 e) among other hydrogen atoms of the studied compound – this confirms the existence of HB interaction between these units.

For such system, the existence of eight mesomeric structures is possible which is presented in Fig. 6. It should be noted that the charge distribution of the MA3MPO molecule, i.e. the induction and mesomeric effects of substituents in pyridine-methylamino skeleton are properly reflected by the theoretical data. While analyzing the calculated Mulliken and NBO charges and mesomeric structures (see Table 5 and Fig. 6), it can be stated that among the presented structures, (7) and (8) are mostly favored.

3.3.2. Electron energy levels

It is expected that the studied compound should give rise to the $\pi \rightarrow \pi^*$ electron transitions usually observed within the range of 190–300 nm. Besides, lone electron pairs located at the nitrogen atoms of the pyridine ring and methylamino group as well as oxygen atom of N-oxide unit should participate in the $n \rightarrow \pi^*$ electron transitions, normally observed within the range of 250–600 nm These two types of electron absorptions should be observed in the form of separate multiplets in the UV-VIS range. The calculated energies of the filled Molecular Orbitals for the studied compound are shown in Fig. 7. The theoretical HOMO → LUMO energy gap equals to 4.48 eV (36140.88 cm^{-1}), i.e. at $\lambda = 276$ nm. Such a picture suggests that in the HOMO → LUMO excitation the low electron pair of the oxygen atom of the NO group is transferred to π^* antibonding orbitals of the pyridine ring.

The conjugated molecules exhibit a small energy gap between the highest occupied molecular orbital HOMO and the lowest unoccupied molecular orbital LUMO. This is the result of a significant degree of intramolecular charge transfer (ICT) from the end capping electron-donor groups to the efficient electron-acceptor groups through π-conjugated path. HOMO level, lying at −5.67 eV, is localized on (lone pair) orbital of the oxygen atom of the NO group, whereas the LUMO level of the energy −1.19 eV is π^* orbital localized on the pyridine ring. Electron transfer occurs from the electron-donor oxygen atom of the NO group to the electron-withdrawing part of pyridine ring. The HOMO–LUMO energy gap in MA3MPO, calculated at the B3LYP/6-311++G(d,p) level, equals to 4.48 eV. Such HOMO–LUMO energy gap originates from the large stabilization of the LUMO orbital due to the strong electron-acceptor ability of the pyridine ring.

3.3.3. Natural bond orbital analysis

NBO analysis has been performed for MA3MPO at the DFT/B3LYP level using the NBO 3.1 program that is part of the Gaussian 03 package. It was expected that these evaluations would allow for

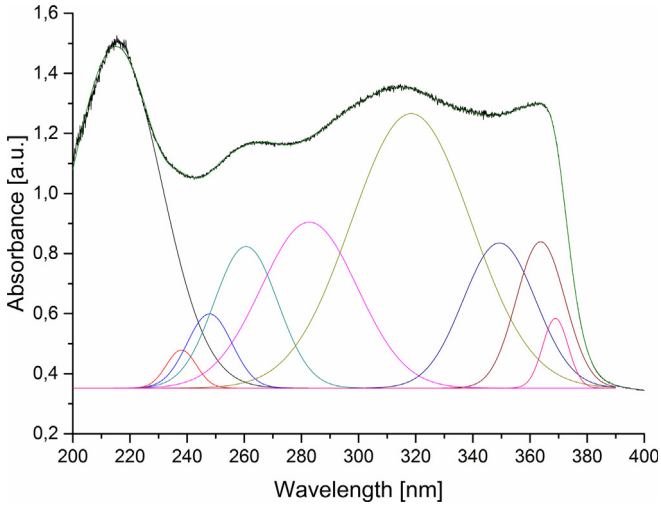

Fig. 7. The UV absorption spectrum of MA3MPO with its deconvolution into Gaussian components.

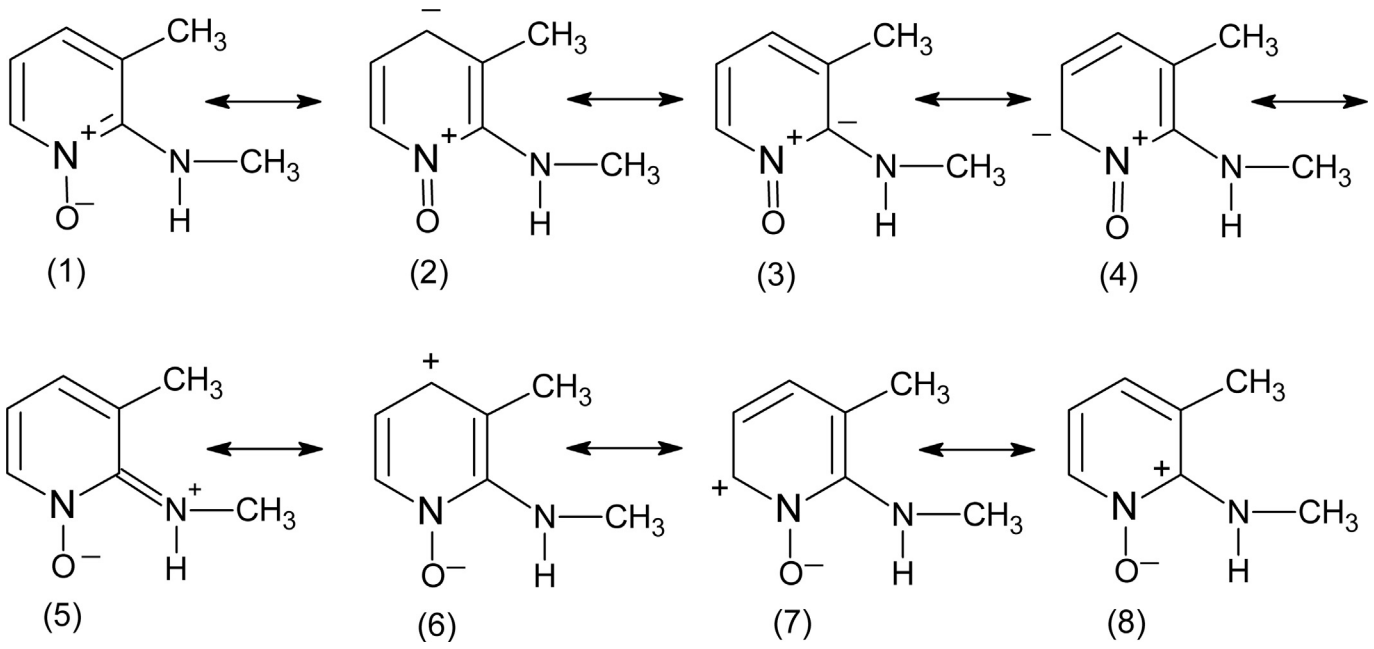

Fig. 6. The resonance structures of the MA3MPO molecule.

characterization of the role of the intramolecular hydrogen bond in stabilizing the structure and delocalization of electron density within the molecule. One of the methods for determination of energy and some properties of hydrogen bonds is the natural bonded orbitals method (NBO) [65–68]. The existence of the intramolecular hydrogen bond in the MA3MPO molecule is confirmed by the NBO presented in Table 6. It follows from the parameters characterizing interaction between the oxygen lone pair of the N-oxide group and N–H antibonding orbital of the amino group (LP (2) O2→σ*N2–H2). Although the energetic contribution (6.55 kcal/mol) of hyperconjugative interactions is not significant, the $E^{(2)}$ value has chemical significance, and can be used as a measure of the intra-molecular electron delocalization in the molecule. The medium binding the strength of an intramolecular hydrogen bond is also confirmed by the high value of electron density (ED = 0.03610 e) on the σ*N–H orbital (Table 6). While analysing the energies that follow from the second-order perturbation theory of Fock matrix strong intra-molecular hyperconjugative interactions are seen. The $E^{(2)}$ (donor → acceptor) energies are significant for the π*(C2–N1) bond and the values shown in Table 5 prove that the intra-molecular hyperconjugative interactions result from the orbital overlap between the π(C–C and C – N) and π*(C–C and C – N) bond orbitals. This intra-molecular charge transfer (ICT) causes stabilization of whole system. Clear decrease in electron density within the range of Ed = 1.68524–1.72411 e is observed on the π binding orbitals of the pyridine ring and, simultaneously, increase of electron density on the respective π* antibonding orbitals is observed.

The important interaction energy, related to the resonance in the molecule, is electron donation from lone pairs of the oxygen atom of the N-oxide group LP (2) O1 to the antibonding acceptors σ*(C2 – N1), σ*(C6 – N1) and, especially, from orbital LP(3) O1 to π*(C2 – N1) of the MA3MPO ($E^{(2)}$ = 38.55 kcal/mol). These interactions are observed as an increase in electron density (ED = 0.06291, 0.03601 and 0.64336 e) in the σ*(C – N) and π*(C – N) antibonding orbitals, respectively and a decrease in electron density (ED = 1.91494 and 1.72492 e) in n orbitals (see Table 6). Higher interaction energy $E^{(2)}$ is observed for electron donation from lone pair of the amino nitrogen atom LP(1) N2 to the antibonding acceptor π*(C2 – N1) ($E^{(2)}$ = 46.29 kcal/mol).

3.3.4. UV –VIS absorption spectra

The electron absorption spectrum of the studied compound was recorded at room temperature in the solid state (Nujol mull). The spectrum is shown in Fig. 7. The contour observed within the range of 200–400 nm has been deconvoluted into nine Gaussian components with the maxima at 215, 238, 248, 261, 283, 318, 349, 364, 389 nm. The assignment of these wavelengths to the respective electron transitions was made on the basis of time depended TD-DFT method. The results of these evaluations are listed in Table 7 in which the energies of ten singlet and triplet states, oscillator strength and main contributions are summarized. The singlet states were localized at the following wavenumbers: S_1 32363; S_2 35840 S_3 36232; S_4 38168; S_5 40161; S_6 41494; S_7 42735; S_8 43290; S_9 43860 and S_{10} 44643 cm^{-1} and those of triplet states: at T_1 20161; T_2 28409 and T_3 29762 cm^{-1}. The respective electron transitions should be assigned to the following wavelength ranges: $\pi \rightarrow \pi^*$ at 190–220 nm; $n(O) \rightarrow \pi^*$ at 230–255 nm; $n(N_{pyridine}) \rightarrow \pi^*$ at 280–300 nm and $n(N_{amine}) \rightarrow \pi^*$ at 320–420 nm. The calculated energies of electron transitions are in good agreement with those reported in our earlier papers on other pyridine derivatives [42,69–72].

3.3.5. Emission spectra

The emission spectrum of the studied compound was measured in the solid state. It contains a very broad contour with the maximum at about 580 nm (Fig. 8). It is clearly shifted into red in relation to the $S_0 \rightarrow S_1$ absorption transition. The observed contour probably originates from T_1,$T_2 \rightarrow S_0$ emission that may proceed by the inter-system crossing $S_1 \rightarrow T_1$,T_2 transition. Room temperature fluorescence is generally not observed from excited triplet states, however, having in mind the calculated energies of the Molecular Orbitals, we believe that such character of this transition is reasonable. According to the DFT calculations, the energies of the T_1 and T_2 states are 20161 cm^{-1} and 28409 cm^{-1}, respectively, i.e. are close to those expected for the emission from the triplet state. The small energetic splitting between these levels probably causes overlapping of these bands in the form of broad T_1-T_2 contour. Besides, their red shift agrees with the expectations because both intra- and inter-molecular hydrogen bonds significantly affects the excited state properties. The excited-state hydrogen bonding influences nonadiabatic processes like internal conversion,

Table 6
Second order perturbation theory analysis of the Fock Matrix in the NBO basis for selected NBO pairs of MA3MPO, obtained from the B3LYP/6-311++G(d, p) calculations.

Donor (i)	ED [e]	Acceptor (j)	ED [e]	$E^{(2)}$ [kcal/mol]	$E_{(j)}$ - $E_{(i)}$ [a.u.]	$F_{(i,j)}$ [a.u.]
π(C2 – N1)	1.72411	π*(C3 – C4)	0.36537	9.41	0.38	0.054
		π*(C5 – C6)	0.32930	20.62	0.37	0.079
π(C3 – C4)	1.68524	π*(C2 – N1)	0.64336	32.30	0.20	0.079
		π*(C5 – C6)	0.32930	18.85	0.28	0.065
π(C5 – C6)	1.7170	π*(C2 – N1)	0.64336	12.51	0.22	0.051
		π*(C3 – C4)	0.36537	19.28	0.30	0.069
σ(N2–H2)	1.97756	σ*(C2 – C3)	0.02925	5.78	1.16	0.073
LP(2) O1	1.91494	δ*(C2 – N1)	0.06291	7.75	0.66	0.064
		δ*(C6 – N1)	0.03601	8.63	0.71	0.071
		δ*(N2–H2)	0.03610	6.55	0.67	0.060
LP(3) O1	1.72492	π*(C2 – N1)	0.64336	38.55	0.18	0.082
LP(1) N2	1.75774	π*(C2 – N1)	0.64336	46.29	0.22	0.100
		δ*(C7–H7a)	0.00897	6.73	0.66	0.063
π*(C2 – N1)	0.64336	π*(C3 – C4)	0.36537	63.45	0.08	0.091
		π*(C5 – C6)	0.32930	34.42	0.07	0.065

Atom numbering is the same as presented in Fig. 1. LP = lone electron pair orbital. The table presents the $E^{(2)}$ values greater than 5 kcal/mol, $E^{(2)}$ – denotes the hyperconjugative interactions, $E_{(j)} - E_{(i)}$ is the energy difference between donor (i) and acceptor (j) orbitals, F(i,j) is the Fock matrix element between i and j NBO orbitals.

Table 7
Experimental and theoretical electronic transitions (with only major contribution) and oscillator strength for MA3MPO (H denotes the HOMO and L the LUMO orbitals).

No	Singlet Excited States				No	Triplet Excited States		
	Exp.	Calculated				Exp.	Calculated	
	λ [nm] [cm^{-1}]	λ [nm] [cm^{-1}]	Oscillator strength	Main contri-bution		λ [nm] [cm^{-1}]	λ [nm] [cm^{-1}]	Main contri-bution
S_1	318 *31446*	310 *32363*	0.0518	H → L+1	T_1	369 *27174*	496.9 *20161*	H → l
S_2	283 *35461*	279 *35840*	0.0618	H → L+1	T_2	364 *27548*	352.7 *28409*	H → L+1
S_3		277 *36232*	0.0117	H-2 → L	T_3	349 *28653*	336.2 *29762*	H-1 → L
S_4	261 *38461*	263 *38168*	0.0270	H → L+2	T_4		293.8 *34130*	H-2 → L
S_5	248 *40486*	250 *40161*	0.0110	H → L+3	T_5		284.4 *35211*	H-1 → L
S_6		241 *41494*	0.2163	H-1 → L	T_6		267.7 *37453*	H → L+2
S_7	238 *42017*	235 *42735*	0.0142	H → L+4	T_7		251.0 *39841*	H → L+3
S_8		232 *43290*	0.0124	H-2 → L+1	T_8		236.5 *42373*	H → L+4
S_9	215 *46512*	228 *43860*	0.0825	H-1 → L+1	T_9		234.7 *42735*	H-2 → L+1
S_{10}		225 *44643*	0.0194	H → L+4	T_{10}		227.7 *44053*	H → L+4

intersystem crossing, intramolecular charge transfer and photoinduced electron transfer [73–79]. It should be noted that the Stokes shift for the studied sample is close to 8.250 cm^{-1}. Fig. 9 represents the system of ten singlet and three triplet states of MA3MPO.

The theoretical DFT calculations and experimental data show that for the studied compound the energy of the singlet states appears within the range of 309 nm (32,360 cm^{-1}) – 224 nm (44,645 cm^{-1}), and for the triplet states within the range of 490 nm (20,160 cm^{-1}) – 330 nm (29,765 cm^{-1}). These energy levels fit well those of europium(III) and terbium(III) ions, forming complexes for molecular imaging and sensing applied in chemical, biological and biomedical sciences [73–79].

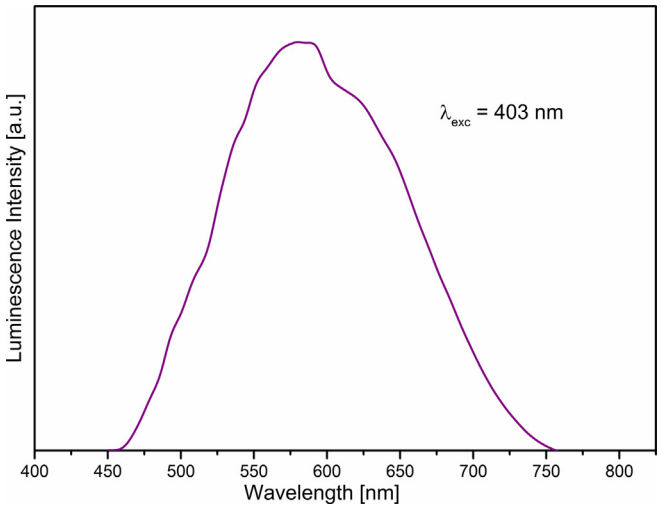

Fig. 8. The experimental luminescence spectrum of MA3MPO.

4. Conclusions

1. 2-N-methylamino-3-methylpyridine N-oxide (MA3MPO) is a new compound for which we expect several prospective applications. It crystallizes in monoclinic $P2_1/n$ structure, and conformation of the MA3MPO molecule is stabilized by the intra-molecular N–H···O (2.527 Å and 120°) hydrogen bond, between the hydrogen atom of the amine group and the oxygen atom of the N-oxide group. The respective geometrical parameters (2.539 Å and 118°) obtained in the DFT quantum chemical calculations are close to experimental values.
2. The experimental N–O bond length (1.334 Å) is slightly longer than the calculated distance (1.298 Å) as well as those reported earlier for 2-alkylaminopyridine N-oxides (1.301–1.318 Å). This effect follows from the participation of this bond in the HB interactions. The X-ray studies also postulate the existence of weak C–H···O contacts between the N-oxide as acceptors and the H atoms of the pyridine and the methyl groups as donors. However, the IR and Raman spectra as well as the quantum chemical calculations do not confirm the presence of such interactions.
3. The quantum-chemical calculations conducted for isolated MA3MPO molecules locate the lowest singlet state assigned to the n → π* (CT) transitions overlapped with some contribution of the π → π* intramolecular charge transfer (ICT). The energy gap between these electron levels forms a specific sequence that may be applied for the ligand to lanthanide ion energy transfer. The depopulation mechanism of the excited states for the studied pyridine N-oxide is proposed.
4. The N-oxide group substituted to the pyridine ring can act effectively as an electron donor and an electron acceptor at the same time. For these reasons, the studied compound appears as a synthetic intermediate in the field of heterocyclic chemistry, protecting group, auxiliary agent, catalysts, and as complexing ligands for d- and f-metal ions. In particular, the MA3MPO could be used as a complexing ligand of europium and terbium ions in the luminescent probes of biological and medical applications.

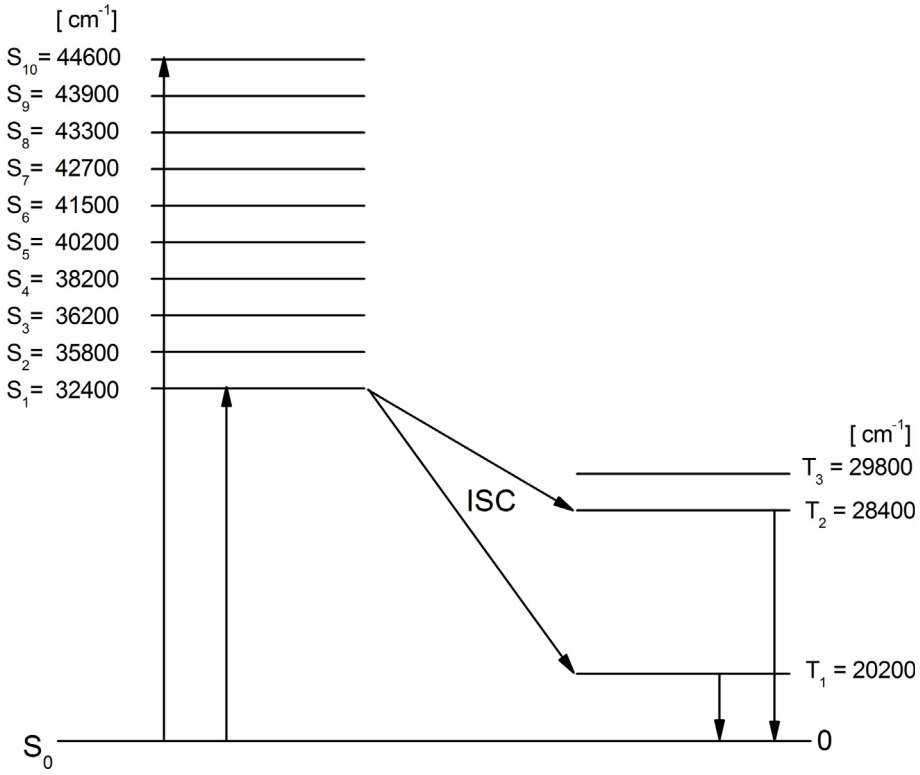

Fig. 9. Depopulation mechanism of the excited states proposed for MA3MPO.

Acknowledgement

The presented work was partially supported by: Polish Ministry of Science and Higher Education under the statutory investigations at the Department of the Bioorganic Chemistry, Wrocław University of Economics and the Department of Drugs Technology, Faculty of Pharmacy with Division of Laboratory Diagnostics, Wroclaw Medical University, and also by the Polish National Centre of Science under grant No. 2014/15/B/ST5/04730.

References

[1] P.M. Dewick, Medicinal Natural Products: A Biosynthetic Approach, second ed., John Wiley & Sons Ltd., John Wiley & Sons Ltd, Chichester, 2002.
[2] H. Hagenmaier, A. Keckeisen, W. Dehler, H.P. Fiedler, H. Zahner, W.A. König, Liebigs Ann. Chem. 6 (1981) 1018–1024. https://doi.org/10.1002/jlac.198119810607.
[3] H. Nishioka, T. Sawa, Y. Takahashi, H. Naganawa, M. Hamada, T. Takeuchi, J. Antibiot. 46 (1993) 564–568. https://doi.org/10.7164/antibiotics.46.564.
[4] M. Stadler, F. Bauch, T. Henkel, A. Mühlbauer, H. Müller, F. Spaltmann, K. Weber, Arch. Pharm. Pharm. Med. Chem. 334 (2001) 143–147. https://doi.org/10.1002/1521-4184, 200105)334:5<143::AID-ARDP143>3.0.CO;2-B.
[5] R.P. Maskey, F. Huth, I. Grün-Wollny, H. Laatsch, Z. Naturforsch. 60b (2005) 63–66.
[6] A.-R.B.A. El-Gazzar, H.A.R. Hussein, H.N. Hafez, Acta Pharm. 57 (2007) 395–411. https://doi.org/10.2478/v10007-007-0032-6.
[7] M.H. Hsu, Ü. Savas, J.M. Lasker, E.F. Jonson, J. Pharmacol. Exp. Ther. 337 (2011) 125–136. https://doi.org/10.1124/jpet.110.175851.
[8] A.M.R. Bernardino, A.R. de Azevedo, L.C.d.S. Pinheiro, J.C. Borges, V.L. Carvalho, M.D. Miranda, M.D.F. de Meneses, M. Nascimento, D. Ferreira, M.A. Rebello, V.A.G.G.d. Silva, I.C.P.P. de Frugulhetti, Med. Chem. Res. 16 (2007) 352–369. https://doi.org/10.1007/s00044-007-9035-6.
[9] N.Y. Wang, W.Q. Zuo, Y. Xu, C. Gao, X.X. Zeng, L.D. Zhang, X.Y. You, C.T. Peng, Y. Shen, S.Y. Yang, Y.Q. Wei, L.T. Yu, Bioorg. Med. Chem. Lett 24 (2014) 1581–1588. https://doi.org/10.1016/j.bmcl.2014.01.075.
[10] A.K. Elansary, A.A. Moneer, H.H. Kadry, E.M. Gedawy, Arch Pharm. Res. (Seoul) 35 (2012). https://doi.org/10.1007/s12272-012-1107-6.
[11] A. Lauria, L. Abbate, C. Patella, A. Martorana, G. Dattolo, A.M. Almerico, Eur. J. Med. Chem. 62 (2013) 416–424. https://doi.org/10.1016/j.ejmech.2013.01.019.
[12] R.M. Mohareb, F. Al-Omran, R.A. Azzam, Steroids 84 (2014) 46–56. https://doi.org/10.1016/j.steroids.2014.03.012.
[13] A.R. Nikkhoo, R. Miri, N. Arianpour, O. Firuzi, A. Ebadi, A.A. Salarian, Med. Chem. Res. 23 (2014) 1225–1233. https://doi.org/10.1007/s00044-013-0729-7.
[14] S.A. Ahmed, O.M. Ahmed, H.S. Elgendy, J. Pharm. Res. 8 (2014) 1303–1313.
[15] E.A. Bakhite, A.E. Abdel-Rahman, O.S. Mohamed, E.A. Thabet, Pharmazie 55 (2000) 577–583.
[16] F.M.A. Altalbawy, Int. J. Mol. Sci. 14 (2013) 2967–2979. https://doi.org/10.3390/ijms14022967.
[17] N.N. Bumpus, E.F. Jonson, J. Pharmacol. Exp. Ther. 339 (2011) 886–896. https://doi.org/10.1124/jpet.111.184242.
[18] K.J. Peyton, X.M. Liu, Y. Yu, B. Yates, W. Durante, J. Pharmacol. Exp. Ther. 342 (2012) 827–834. https://doi.org/10.1124/jpet.112.194712.
[19] K. Nakajiama, Y. Komiyama, H. Hojo, S. Ohba, F. Yano, N. Nishikawa, H. Aburatani, T. Takato, U. Chung, Biochem. Biophys. Res. Commun. 395 (2010) 502–508. https://doi.org/10.1016/j.bbrc.2010.04.041.
[20] Y. Maeda, H. Hojo, N. Shimohata, S. Choi, K. Yamamoto, T. Takato, U. Chung, S. Ohba, Biomaterials 34 (2013) 5530–5537. https://doi.org/10.1016/j.biomaterials.2013.03.089.
[21] T. Gemba, M. Ninomiya, K. Matsunaga, M. Ueda, J. Pharmacol. Exp. Ther. 265 (1993) 463–467.
[22] M. Ishihara, T. Tsuneya, M. Shiga, H. Sato, F. Yoshida, K. Yamagishi, Patent No. US005214027A, http://www.freepatentsonline.com/5214027.html.
[23] J. Balzarini, M. Stevens, G. Andrei, R. Snoeck, R. Strunk, J.B. Pierce, J.A. Lacadie, E. De Clercq, C. Pannecouque, Helv. Chim. Acta 85 (2002) 2961–2974. https://doi.org/10.1002/1522-2675(200209)85:9<2961::AID-HLCA2961>3.0.CO;2-R.
[24] M. Stevens, C. Pannecouque, E. De Clercq, J. Balzarini, Antimicrob. Agents Chemother. 47 (2003) 2951–2957. https://doi.org/10.1128/AAC.47.9.2951–2957.2003.
[25] M. Stevens, C. Pannecouque, E. De Clercq, J. Balzarini, Antimicrob. Agents Chemother. 47 (2003) 3109–3116. https://doi.org/10.1128/AAC.47.10.3109–3116.2003.
[26] J. Balzarini, M. Stevens, E. De Clercq, D. Schols, C. Pannecouque, J. Antimicrob. Chemother. 55 (2005) 135–138. https://doi.org/10.1093/jac/dkh530.
[27] E.F.V. Scriven, R. Murugan, Pyridine and pyridine derivatives, in: Kirk-Othmer Encyclopedia of Chemical Technology, vol. 20, John Wiley & Sons, Inc., 2005, pp. 1–53. https://doi.org/10.1002/0471238961.1625180919031809.a01.pub2.
[28] C. Liu, J. Luo, L. Xu, Z. Huo, Arcivoc (i) (2013) 154–174. https://doi.org/10.3998/ark.5550190.0014.105.
[29] F. Dzierszinski, A. Coppin, M. Mortuaire, E. Dewailly, C. Slomianny, J.C. Ameisen, F. DeBels, S. Tomavo, Antimicrob. Agents Chemother. 46 (2002) 3197–3207. https://doi.org/10.1128/AAC.46.10.3197-3207.2002.
[30] H. Dressler, Pyridine and derivatives, in: D.M. Considine, G.D. Considine (Eds.),

Van Nostrand's Scientific Encyclopedia Van Nostrand's Scientific Encyclopedia, John Wiley & Sons, Inc., 2006. https://doi.org/10.1002/0471743984.vse5857.
[31] J. Balzarini, E. Keyaerts, L. Vijgen, F. Vandermeer, M. Stevens, E. De Clercq, H. Egberink, M. Van Ranst, J. Antimicrob. Chemother. 57 (2006) 472–481. https://doi.org/10.1093/jac/dki481.
[32] S. Youssif, Arkivoc (i) (2001) 242–268.
[33] S.N. Kilényi, J.J. Mousseau, Pyridine N-oxide, in: Encyclopedia of Reagents for Organic Synthesis, John Wiley & Sons, Ltd., 2015, p. 1. https://doi.org/10.1002/047084289X.rp283.pub2.
[34] R.L. Carlin, J. Am. Chem. Soc. 83 (1961) 3773–3775. https://doi.org/10.1021/ja01479a010.
[35] R. Sarma, A. Karmakar, J.B. Baruah, Inorg. Chim. Acta 361 (2008) 2081–2086. https://doi.org/10.1016/j.ica.2007.10.029.
[36] J. Lorenc, I. Bryndal, W. Syska, M. Wandas, M. Marchewka, A. Pietraszko, T. Lis, M. Mączka, K. Hermanowicz, J. Hanuza, Chem. Phys. 374 (2010) 1–14. https://doi.org/10.1016/j.chemphys.2010.05.013.
[37] I. Bryndal, E. Kucharska, W. Sąsiadek, M. Wandas, T. Lis, J. Lorenc, J. Hanuza, Spectrochim. Acta A 96 (2012) 952–962. https://doi.org/10.1016/j.saa.2012.07.121.
[38] J. Lorenc, Vib. Spectrosc. 61 (2012) 112–123. https://doi.org/10.1016/j.vibspec.2012.03.006.
[39] I. Bryndal, M. Marchewka, M. Wandas, W. Sąsiadek, J. Lorenc, T. Lis, L. Dymińska, E. Kucharska, J. Hanuza, Spectrochim. Acta A 123 (2014) 342–351. https://doi.org/10.1016/j.saa.2013.12.018.
[40] I. Bryndal, E. Kucharska, M. Wandas, J. Lorenc, K. Hermanowicz, M. Mączka, T. Lis, M. Marchewka, J. Hanuza, Spectrochim. Acta A 117 (2014) 434–441. https://doi.org/10.1016/j.saa.2013.08.038.
[41] E. Lorenz, M. Mączka, K. Hermanowicz, A. Waśkowska, A. Puszko, J. Hanuza, Vib. Spectrosc. 37 (2005) 195–207. https://doi.org/10.1016/j.vibspec.2004.09.003.
[42] J. Lorenc, J. Hanuza, J. Janczak, Vib. Spectrosc. 59 (2012) 59–70. https://doi.org/10.1016/j.vibspec.2012.01.003.
[43] Z. Talik, A. Puszko, Prace Naukowe A. E. Wrocław 238 (1983) 107–111.
[44] CrysAlis CCD and CrysAlis RED Programs, Oxford Diffraction Ltd., Yarnton, Oxfordshire, England, 2010.
[45] G.M. Sheldrick, Acta Crystallogr. A 64 (2008) 112–122. https://doi.org/10.1107/S0108767307043930.
[46] G.M. Sheldrick, Acta Crystallogr. C 71 (2015) 3–8. https://doi.org/10.1107/S2053229614024218.
[47] K. Brandenburg, DIAMOND Version 3.0, Crystal Impact GbR, Bonn, Germany, 2014.
[48] S. Nunn, K. Nishikida, Thertmo Fisher Scientific, Madison, WI, USA.
[49] M.J. Frisch, G.W. Trucks, H.B. Schlegel, G.E. Scuseria, M.A. Robb, J.R. Cheeseman, J.A. Montgomery, T. Vreven Jr., K.N. Kudin, J.C. Burant, J.M. Millam, S.S. Iyengar, J. Tomasi, V. Barone, B. Mennucci, M. Cossi, G. Scalmani, N. Rega, G.A. Petersson, H. Nakatsuji, M. Hada, M. Ehara, K. Toyota, R. Fukuda, J. Hasegawa, M. Ishida, T. Nakajima, Y. Honda, O. Kitao, H. Nakai, M. Klene, X. Li, J.E. Knox, H.P. Hratchian, J.B. Cross, C. Adamo, J. Jaramillo, R. Gomperts, R.E. Stratmann, O. Yazyev, A.J. Austin, R. Cammi, C. Pomelli, J.W. Ochterski, P.Y. Ayala, K. Morokuma, G.A. Voth, P. Salvador, J.J. Dannenberg, V.G. Zakrzewski, S. Dapprich, A.D. Daniels, M.C. Strain, O. Farkas, D.K. Malick, A.D. Rabuck, K. Raghavachari, J.B. Foresman, J.V. Ortiz, Q. Cui, A.G. Baboul, S. Clifford, J. Cioslowski, B.B. Stefanov, G. Liu, A. Liashenko, P. Piskorz, I. Komaromi, R.L. Martin, D.J. Fox, T. Keith, M.A. Al-Laham, C.Y. Peng, A. Nanayakkara, M. Challacombe, P.M.W. Gill, B. Johnson, W. Chen, M.W. Wong, C. Gonzalez, J.A. Pople, Gaussian 03, Revision A.1, Gaussian, Inc., Pittsburgh PA, 2003.
[50] A.D. Becke, J. Chem. Phys. 104 (1996) 1040–1046. https://doi.org/10.1063/1.470829.
[51] C. Lee, W. Yang, R.G. Parr, Phys. Rev. B 37 (1988) 785–789. https://doi.org/10.1103/PhysRevB.37.785.
[52] R.G. Parr, W. Yang, Density-functional Theory of Atoms and Molecules, Oxford University Press, New York, 1989.
[53] A.D. McLean, J. Chem. Phys. 72 (1980) 5639–5648. https://doi.org/10.1063/1.438980.
[54] R. Krishnan, J.S. Binkley, R. Seeger, J.A. Pople, J. Chem. Phys. 72 (1980) 650–654. https://doi.org/10.1063/1.438955.
[55] M.J. Nowak, L. Lapinski, H. Rostkowska, L. Lapinski, M.J. Nowak, BALGA computer program for PED calculations, Vib. Spectrosc. 49 (2009) 43–51. https://doi.org/10.1016/j.vibspec.2008.04.012.
[56] G.A. Andrienko, ChemCraft (Build 486), Version 1.8. www.chemcraftprog.com.
[57] M.A. Palafox, V.K. Rastogi, Spectrochim. Acta A 58 (2002) 411–440. https://doi.org/10.1016/S1386-1425(01)00509-1.
[58] Ł. Wiśniewski, A. Urbanowicz, L. Jerzykiewicz, A. Makarewicz, I. Deprasińska, G. van der Zwan, N. Haraszkiewicz, A. Puszko, A. Szemik-Hojniak, J. Mol. Struct. 920 (2009) 45–51. https://doi.org/10.1016/j.molstruc.2008.10.029.
[59] A. Szemik-Hojniak, I. Deperasińska, L. Jerzykiewicz, P. Sobota, M. Hojniak, A. Puszko, N. Harszkiewicz, G. van der Zwan, P. Jacques, J. Phys. Chem. 110 (2006) 10690–10698. https://doi.org/10.1021/jp062405x.
[60] A. Szemik-Hojniak, Ł. Wiśniewski I. Deperasińska, A. Makarewicz, L. Jerzykiewicz, A. Puszko, Y. Erez, D. Huppert, Phys. Chem. Chem. Phys. 14 (2012) 8147–8159. https://doi.org/10.1039/C2CP40591A.
[61] F. Partal Ureña, M. Fernández Gómez, J.J. López Gonzáles, E. Martínez Torres, Spectrochim. Acta A 59 (2003) 2815–2839. https://doi.org/10.1016/S1386-1425(03)00082-9.
[62] K.B. Wilberg, V.A. Walters, K.N. Wong, S.D. Colson, J. Phys. Chem. 88 (1984) 6067–6075. https://doi.org/10.1021/j150668a067.
[63] S. Bratos, J. Lascombe, A. Novak, in: H. Ratajczak, W.J. Orville-Thomas (Eds.), Molecular Interactions, John Wiley & Sons, Chichester, New York, 1980, pp. 301–346.
[64] G.R. Desiraju, T. Steiner, The Weak Hydrogen Bond in Structural Chemistry and Biology, Oxford University Press, Oxford, 1999.
[65] A.E. Reed, F. Weinhold, J. Chem. Phys. 78 (1983) 4066–4073. https://doi.org/10.1063/1.445134.
[66] A.E. Reed, R.B. Weinstock, F. Weinhold, J. Chem. Phys. 83 (1985) 735–746. https://doi.org/10.1063/1.449486.
[67] A.E. Reed, F. Weinhold, J. Chem. Phys. 83 (1985) 1736–1740. https://doi.org/10.1063/1.449360.
[68] J.E. Carpenter, F. Weinhold, J. Mol. Struct.-Theochem 169 (1988) 41–62. https://doi.org/10.1016/0166-1280(88)80248-3.
[69] J. Lorenc, A. Puszko, Chem. Pap. 52 (1998) 756–761.
[70] J. Lorenc, E. Kucharska, J. Michalski, J. Hanuza, E. Mugeński, H. Chojnacki, J. Mol. Struct. 614 (2002) 257–266. https://doi.org/10.1016/S0022-2860(02)00259-4.
[71] J. Lorenc, E. Kucharska, J. Hanuza, H. Chojnacki, J. Mol. Struct. 707 (2004) 47–57. https://doi.org/10.1016/j.molstruc.2004.05.029.
[72] J. Lorenc, J. Mol. Struct. 748 (2005) 91–100. https://doi.org/10.1016/j.molstruc.2005.03.017.
[73] M.S. Masoud, S.S. Hagagg, A.E. Ali, N.M. Nasr, Spectrochim. Acta A 94 (2012) 256–264. https://doi.org/10.1016/j.saa.2012.03.037.
[74] G.H. Dieke, in: H.M. Crosswhite, H. Crosswhite (Eds.), Spectra and Energy Levels of Rare Earth Ions in Crystals, John Wiley, 1968.
[75] E. Soini, T. Lövgren, C.B. Reimer, Crit. Rev. Anal. Chem. 18 (1987) 105–154. https://doi.org/10.1080/10408348708542802.
[76] J.C.G. Bünzli, G.R. Choppin (Eds.), Lanthanide Probes in Life, Chemical and Earth Sciences: Theory and Practice, Elsevier, Amsterdam, 1989, 978-044488199.
[77] L. Hemmilä, V. Laitala, J. Fluoresc. 15 (4) (2005) 529–542. https://doi.org/10.1007/s10895-005-2826-6.
[78] S. Pandya, J. Yu, D. Parker, Dalton Trans. (2006) 2757–2766. https://doi.org/10.1039/B514637B.
[79] M.C. Heffern, L.M. Matosziuk, T.J. Meade, Chem. Rev. 114 (8) (2014) 4496–4539. https://doi.org/10.1021/cr400477t.